Use of the Sampling Theorem to Speed Up Near-Field Physical Optics Scattering Calculations

P. W. Cramer and W. A. Imbriale

Ground Antennas and Facilities Engineering Section

Physical optics scattering calculations performed on the DSN 34-m beam-waveguide antennas at Ka-band (32 GHz) require approximately 12 hr of central processing unit time on a Cray Y-MP2 computer. This is excessive in terms of resource utilization and turnaround time. Typically, the calculations involve five surfaces, and the calculations are done two surfaces at a time. The sampling theorem is used to reduce the number of current values that must be calculated over the second surface by performing a physical optics integration over the first surface. The additional number of current values required on the second surface by subsequent physical optics integrations is obtained by interpolation over the original current values. Time improvements on the order of a factor of 2 to 4 were obtained for typical scattering pairs.

I. Introduction

The technique discussed here was developed to reduce the amount of time required by physical optics to compute the antenna patterns of the 34-m beam-waveguide antennas at the DSN. Figure 1 illustrates a typical DSN beam-waveguide (BWG) antenna. As can be seen, the antenna has eight scattering surfaces. Beginning with the feed system in the pedestal room, there is a flat mirror, an ellipse, a second flat mirror, two parabolas, a third flat mirror, the subreflector and the main reflector. However, the flat mirrors are assumed not to affect the antenna pattern properties and are ignored in the analysis, leaving five scattering surfaces. With this number of mirrors, the analysis must be repeated four times before the final far fields are evaluated. For analysis up to X-band (8.45 GHz), the available computers could easily handle calculations of such size and complexity. However, with the shift to Ka-band (32 GHz) to support future deep-space missions,

computational times are increased by a factor of about 16. Computational times of 12 hr on a Cray Y-MP2 single processor computer are typical.

This article presents a method to reduce the overall time by a factor of 4 or more for a typical pair of scattering surfaces and by a factor of 2 for the overall antenna system. The sampling theorem coupled with a near-field radial interpolation algorithm is used to speed up the physical optics calculations.

The sampling theorem has been used previously for the far-field analysis of reflecting surfaces [1]. A sampling-like technique [2] that allows the use of the Fast Fourier Transform (FFT) algorithm has been used to calculate the far fields of a parabolic reflector and the Fresnel zone fields of a planar aperture. Both methods [1] and [2] were extended to the near field [3,4], but were limited to calculating the fields on a spherical surface of constant radius.

Evaluating a BWG system requires multiple near-field calculations on arbitrary surfaces. To overcome the existing limitations, the sampling technique has been generalized for *arbitrary* field point calculations in the near field. Also, since evaluations on multiple surfaces are required, a technique is outlined for developing an equivalent source aperture that defines the geometry required to calculate the optimum sampling parameters.

II. Method

The basic method used to analyze the 34-m antennas consisted of performing a physical optics integration over the currents on the various surfaces of the antenna. The form of the physical optics program used here [5] is based upon a discrete approximation of the radiation integral. In this approach, the reflector surface is replaced by a triangular facet representation such that the surface resembles a geodesic dome. The physical optics currents are assumed to be constant in amplitude and phase over each of the facets so the radiation integral is reduced to a simple summation of the contributions of each facet.

To evaluate the complete antenna, an integration is performed over the currents on the first scattering surface to get the currents on the second surface. Using these new currents on the second surface, the process is repeated for the next surface, continuing the utilization of pairs of surfaces until the complete antenna has been analyzed. The final integration over the main reflector uses the Jacobi-Bessel form of physical optics [6], which is much faster for calculating far-field patterns from large reflectors, but unfortunately not amenable to the use of the sampling theorem. With the exception of the main reflector, if each surface is considered to be of comparable size, and if the required current resolution in any direction is $\mathcal{N}$, then $\mathcal{N}^2$ physical optics integrations are required over the first surface for each of the required $\mathcal{N}^2$ current points on the second scattering surface. This implies $\mathcal{N}^4$ calculations and is the real driver for the computational time.

Assuming first that the number of surface current values that must be calculated using physical optics on the second surface can be reduced significantly, and second that the $\mathcal{N}^2$ current values needed to perform the subsequent physical optics integration can be obtained by interpolating over the reduced surface current set, then the computational time will approach that of $\mathcal{N}^2$ operations on the first surface. The physical optics integral is composed of two basic parts, the current term and the kernel or exponential term. The current term is typically a slowly varying function of position, while the kernel varies rapidly

as a function of position and observation point. The approach is to employ the sampling theorem to calculate the number of surface current values necessary to define the surface currents on the second surface, and then to use an interpolation algorithm to obtain the larger number of points required by the rapidly varying, but easily evaluated kernel.

A key problem is to define a field sampling function that could be used to determine the sampling frequency. Patterns produced by a uniform distribution have the narrowest beamwidths. Any deviations from a uniform distribution broadens the pattern shape or beamwidth. Therefore, the pattern derived from a uniform aperture distribution should have the highest frequency content and should provide a conservative estimator for the maximum sampling frequency. Figure 2 illustrates the far-field pattern distribution that results from a uniformly illuminated square aperture and is defined by the following function in the u direction:

$$E(u) = \frac{\sin(u)}{(u)}$$

where

$$u = \frac{2\pi X_m \sin\theta}{\lambda}$$

X_m = center to edge dimension of a square source aperture in the x direction

θ = angle to a field point on the sampling surface

λ = wavelength

If this distribution is evaluated on the sampling surface, then the distance from the surface center to its edge in (u, v) space is

$$u_m = \frac{2\pi X_m \sin\theta_m}{\lambda}$$

where θ_m = angle to the edge of the sampling surface. $E(v)$ in the orthogonal direction can be defined in a similar manner.

The distribution frequency is

$$B = \frac{u_m}{u_d}$$

where $u_d = 2\pi$ is the distribution period.

Since the sampling theorem requires sampling at twice the highest frequency and includes sampling points over the full width of the sampling surface, the number of sampling points required is

$$N = 2(2B) + 1$$

or

$$N = \frac{4X_m \sin \theta_m}{\lambda} + 1$$

The $\sin(u)/(u)$ function is based on a far-field derivation. Although it does not provide a rigorous basis for estimating the sampling frequency for sampling surfaces in the near field, it still gives a good estimate for typical source aperture fields. Also, the fields on the sampling surface are not a strictly band-limited function. To account for these limitations, an 18-percent oversampling was used, an approach that provides sufficient accuracy (as will be shown later).

Sinc functions are used to do the interpolations and to evaluate the fields at any point on a sampling surface; thus,

$$H_{(u)} = \sum_{n=-N/2}^{N/2} H_{(n)} \frac{\sin(u - n\pi)}{(u - n\pi)}$$

Since the $\sin(u)/(u)$ field function is defined on a spherical surface, the sampling must also be done on a spherical surface. Also, the spherical surface origin must be located at the center of the source aperture. In addition, the origin of the spherical surface must also be at the field function phase center so as to minimize the phase variations over the spherical surface. This implies that the field function phase center must also coincide with the source aperture origin. In general there are three problems: First, the reflector surfaces usually are not spherical; second, even if the reflector surface were spherical, its origin may not be located at the origin of the source aperture; third, the center of the source aperture may not be the phase center of the scattered fields. To accommodate nonspherical surfaces or spherical surfaces with offset phase centers, the sampling surface of interest is enclosed by two spherical surfaces, with the origins of the two surfaces at the phase

center of the scattered fields. Figure 3 illustrates the geometry. In the figure are five surfaces: In addition to the physical source aperture (subreflector), and the ultimate sampling surface (main reflector), there are the two surfaces enclosing the ultimate sampling surface and an equivalent source aperture. If the scattered field phase center does not coincide with the center of the physical source aperture, an equivalent source aperture is constructed at the phase center.

To determine where the phase center should lie, a subset of the scattered field phase pattern is calculated on a spherical surface constructed midway between the two initial spherical reflectors, which have their origins at the center of the physical source aperture. A phase center location is computed that minimizes the phase pattern variations, in a least-squares sense, over the spherical surface. A discussion of this technique is beyond the scope of this article; however, W. Rusch and P. Potter [7] describe a two-dimensional technique that is the basis of the three-dimensional technique used here. The controlling equations are summarized here (see Fig. 4), where R is the radius of the spherical reflector. The objective is to minimize the following function:

$$\sigma = \Sigma w_i \left(kd \cos \gamma_i + c - \Phi_i - \overline{\Delta}\right)^2$$

with minimization conditions:

$$\frac{\delta\sigma}{\delta x_d} = 0$$

$$\frac{\delta\sigma}{\delta y_d} = 0$$

$$\frac{\delta\sigma}{\delta z_d} = 0$$

where

w_i = phase weight

k = propagation constant

$d = (x_d, y_d, z_d)$ computed vector determining phase center location

γ_i = direction to field phase point

c = residual phase of pattern relative to computed phase center location

Φ_i = phase pattern on spherical surface relative to original pattern origin

$\overline{\Delta}$ = mean of $kd \cos \gamma_i + c - \Phi_i$

The phase center algorithm is based on a far-field approximation, i.e., the adjustment to the phase center location must be small compared to the size and radius of the spherical surface on which the phase is evaluated. This limitation is overcome by iterating the algorithm until the last estimate of the required adjustment to the phase center position is smaller than some specified value.

The equivalent aperture size is estimated to produce a field distribution on the sampling surface similar to that produced by the physical source aperture. Referring to Fig. 3, the equivalent aperture size is

$$X_m = \frac{S_f X_e \sin \theta_e}{\sin \theta_m}$$

where

S_f = oversampling parameter

X_m = center-to-edge dimension of the equivalent source aperture in the x direction

X_e = center-to-edge dimension of the physical source aperture (subreflector)

θ_m = angle to the edge of the sampling surface for the equivalent source aperture

θ_e = angle to the edge of the sampling surface for the physical source aperture

Since a square aperture is used, $Y_m = X_m$. This size is used in the calculation of the number of required sample points N.

After the determination of the sampling parameters and geometry and before any interpolations can be performed, the fields H_n must be computed on a square grid over the two spherical surfaces, the size of the grids being determined by the number of sampling points N. The overall interpolation is performed as follows. A radius from the center of the equivalent source aperture (phase center) is constructed to an interpolation point on the ultimate sampling surface of interest and then made to intercept the two spherical surfaces. Polar interpolated fields are computed on the two spherical surfaces at the intersection

points of the radius. The polar interpolation at each of the spherical surfaces is expressed as follows:

$$H_{(u,v)} = \sum_{n_u=-N_u/2}^{N_u/2} \sum_{n_v=-N_v/2}^{N_v/2} H_{(n_u,n_v)}$$

$$\times \frac{\sin(u - n_u \pi)}{(u - n_u \pi)} \frac{\sin(v - n_v \pi)}{(v - n_v \pi)}$$

where

$$u = \frac{2\pi x X_m}{\lambda r}$$

$$v = \frac{2\pi y Y_m}{\lambda r}$$

x = x coordinate of point on surface of interest

y = y coordinate of point on surface of interest

r = radial distance to point on surface of interest

$H_{(u,v)}$ is evaluated at r_1 and r_2 on the two surfaces and the results are defined as H_1 and H_2, respectively. Next, a radial interpolation is performed between these two points to obtain the interpolated field point on the sampling surface of interest. Since a near-field interpolation is required, terms of the order $1/r$ and $1/r^2$ are used. The appropriate equations are as follows:

$$H = \frac{e^{-jkr}}{4\pi r}\left(A_0 + \frac{A_1}{r}\right)$$

where

$$A_0 = \frac{4\pi}{(r_1 - r_2)}\left(r_1^2 H_1 e^{-jkr_1} - r_2^2 H_2 e^{-jkr_2}\right)$$

$$A_1 = \frac{4\pi r_1 r_2}{(r_2 - r_1)}\left(r_1 H_1 e^{-jkr_1} - r_2 H_2 e^{-jkr_2}\right)$$

This process is repeated until all the fields at all of the required points on the sampling surface have been calculated, then the associated currents that are required for the subsequent physical optics calculations can be calculated.

III. Program Design

This section briefly describes the changes required to an existing physical optics program to implement the sampling capability. The existing program is referred to as a POPO program in that it contains a cascaded design that allows the calculation of the scattered pattern from a two-reflector system. In effect, the currents on the first surface are either calculated from a feed pattern or imported from a previous scattering calculation. Then a physical optics integration is performed over the first surface to obtain the currents on a second surface. At this point, two options are available: Output the currents from the second surface to a file so that they might be imported into a second scattering calculation and/or perform a physical optics integration over the second surface to obtain the output scattered fields for the dual-reflector system. Figures 5(a) and 5(b) illustrate the program design. Figure 5(b) shows the lower level program routines for completeness and will not be discussed further.

Figure 5(a) shows three major blocks as follows: (1) the sampling surface (main reflector) routines, (2) the source aperture (subreflector) routines, and (3) the modules required to implement the sampling capability. The subreflector routines represent the first surface and are used to perform a physical optics integration on the first surface for points requested from the main reflector routines, which represent the second surface. The main reflector routines are then used to perform a physical optics integration over the second surface and to calculate the final scattered patterns. In Fig. 5(a), a dotted line labeled "original interconnection" shows the program in its unmodified form. To implement the sampling theorem mode, the only changes required to the original program were (1) break the link between routines INFLDM and SUBFLD and then insert the block of sampling routines, (2) change INFLDM to call sampling routine SMPFLD instead of SUBFLD, (3) change the main reflector routine DATAIN to read in the data parameters that the sampling routines require, and (4) change the main reflector routine DATAO1 to print out the data parameters associated with the sampling routines. Only simple changes to three routines were required. These routines are enclosed by dotted boxes.

Figure 6 shows a sample input data file for the POPO scattering program. The parameters in the box are the only changes required to the data file to support the sampling capability. The parameter SFACT allows changing the oversampling parameter from the default value of 18 percent to some other value. TFACT allows extending the sampling surface beyond its physical boundaries.

XD,YD, and ZD specify the estimated location of the pattern phase center. SUBSW indicates whether the phase center location is defined in main reflector coordinates or subreflector coordinates. PHASW indicates whether the program is to compute an optimum phase center.

This discussion shows the simplicity of the approach and the ease with which it can be integrated into dual-surface physical optics scattering programs.

IV. Results

Figures 7 and 8 show the accuracy of the sampling approach. In the center of each figure, the geometry of the test case is illustrated to include a pair of parabolic mirrors such as used on a typical 34-m beam-waveguide antenna. The first parabola is the source aperture. The second parabola is the sampling surface on which a reduced set of fields are calculated and then interpolated to obtain the total set of fields and hence the currents required by physical optics to calculate the scattered field from the sampling surface. Figure 7 shows two curves describing the fields calculated on the sampling surface, one curve for the fields calculated in the normal manner and a second curve for the case where interpolation is used with a sparse set of sample points. There is a small amount of ripple between the two curves, less than 0.5 dB, but as seen in the Fig. 8, it has a negligible effect on the far fields calculated from the currents associated with the fields on the sampling surface. The curves shown in Fig. 8 are for the far fields calculated by performing a physical optics integration over the currents on the second parabola (sampling surface). One curve uses currents calculated using the sampling theorem and the other curve is based on the normal method where the currents are computed using physical optics integration for all the current points. As can be seen, the two curves are essentially identical over 40 dB. The differences are primarily in the side-lobe region. However, the side-lobe regions do not illuminate the subsequent scattering surfaces and therefore are of no interest in this particular application.

Figure 9 shows a combination of an elliptical source aperture and a parabolic sampling surface. Again, this is typical of a set of mirrors used in a beam-waveguide antenna. This case is different from the previous example in that the location of the phase center was known in the previous case, while in this case it was not. The source of the fields for the ellipse was from a feed with a transverse offset of approximately 8 wavelengths from the nominal focus, making it difficult to predict where the phase center would be for fields scattered from the ellipse. The program

was allowed to compute the location of the phase center starting with an estimated phase center that would be appropriate for a feed at the focus of the ellipse. The phase center had to be shifted by approximately 16 wavelengths. Except for one glitch, there is good agreement over 35 dB. The glitch represents a 1.5-dB error at a point 20 dB below the pattern peak. Some of the error could possibly be attributed to the difficulty of reproducing a pattern that contained some aberrations due to an offset feed.

An investigation was made to determine the effect of the size of the oversampling parameter on the accuracy of the computed scattered patterns. Figure 10 illustrates the effect of the oversampling parameter for a combination of an ellipse and a parabola. The upper 28 dB of the pattern was truncated to give more resolution to the area most affected by the oversampling parameter. As can be seen, a value of 1.18 is sufficient for a dynamic range of 37 dB (28 + 9). Except for the error at the 37-dB relative level, a value of 1.6 followed the main lobe down to at least the 58-dB relative level. As can be seen, larger oversampling values did not help in the side-lobe region. For most applications, performance below 30 dB is not required and the default value of 1.18 should be adequate. It is recommended that convergence tests be run for each general application or class to determine if the default value is adequate, or if a value of the oversampling parameter smaller than the default is desired. It must be pointed out that the computation time is strongly influenced by the size of the oversampling parameter.

The effect of increasing the sampling surface beyond the limits of the actual surface was investigated to see if this would improve the sampling accuracy, especially by better modeling the fields at the edge of the sampling surface. Figure 11 illustrates the case for an ellipse and parabola combination. A factor TFACT was defined and is a ratio of the angle subtended by a extended sampling surface to the angle subtended by the actual sampling surface. Thus TFACT = 1.0 refers to a sampling surface with no change. Except for some slight changes in the side-lobe region, it was found that increasing the sampling surface size had very little effect on pattern accuracy. This parameter did not show much potential and was not pursued further. Since increasing the sampling surface size strongly affects the computation time, a value of 1.0 should be used.

Figure 12 is a summary of the time improvement that was obtained for a calculation on a 34-m beam-waveguide antenna at Ka-band. Included in Fig. 12 is a schematic diagram of the 34-m BWG antenna with the three flat mirrors removed, which is the geometry analyzed and summarized in the figure. The appearance of the ellipse in front of the main reflector has no physical significance, but is what happens when the flat mirrors are removed. The results are shown by mirror pairs, the first mirror being the source mirror and the second mirror being the sampling mirror. The difference in time between the first two cases is easily accounted for. The sampling frequency is based on the size of the source aperture and the subtended angle produced by the sampling surface relative to the source aperture. In the second case the two mirrors are closer together than in the first case, increasing the subtended angle and in turn requiring a higher sampling frequency. See the equation for calculation of N. The improvements ranged between 1.69 and 4.39. The overall improvement up to and including the subreflector is a factor of 2.73. The sampling theorem was not applied to the main reflector calculation, so an improvement factor of 1.0 was assigned. Including the main reflector, a net improvement of 2.05 was obtained, reducing the computation time from 11.55 hr to 5.64 hr.

References

[1] O. M. Bucci, G. Franceschetti, and C. D'Elia, "Fast Analysis of Large Antennas: A New Computational Philosophy," *IEEE Trans. on Antennas and Propagation*, vol. AP-28, no. 3, pp. 306–310, May 1980.

[2] O. M. Bucci, G. Franceschetti, and R. Pierri, "Reflector Antennas Fields: An Exact Aperture-Like Approach," *IEEE Trans. on Antennas and Propagation*, vol. AP-29, no. 4, pp. 580–586, July 1981.

[3] G. D'Elia, G. Leone, R. Pierri, and D. Valentino, "Numerical Evaluation of the Near Field Using Sampling Expansions," *1982 APS Symposium*, vol. 1, pp. 241–244, June 1982.

[4] F. Benici, G. D'Elia, and R. Pierri, "Numerical Evaluation of Fresnel-Zone Fields by Sampling Like Technique," *1982 APS Symposium*, vol. 2, pp. 515–518, June 1982.

[5] W. A. Imbriale and R. Hodges, "Linear Phase Approximation in the Triangular Facet Near-Field Physical Optics Computer Program," *Applied Computational Electromagnetics Society Journal*, vol. 6, no. 2, pp. 74–85, Winter 1991.

[6] Y. Rahmat-Samii and V. Galindo-Israel, "Shaped Reflector Antenna Analysis Using the Jacobi-Bessel Series," *IEEE Trans. on Antennas and Propagation*, vol. AP-28, pp. 425–435, July 1980.

[7] W. V. T. Rusch and P. D. Potter, *Analysis of Reflector Antennas*, New York: Academic Press, pp. 145–153, 1970.
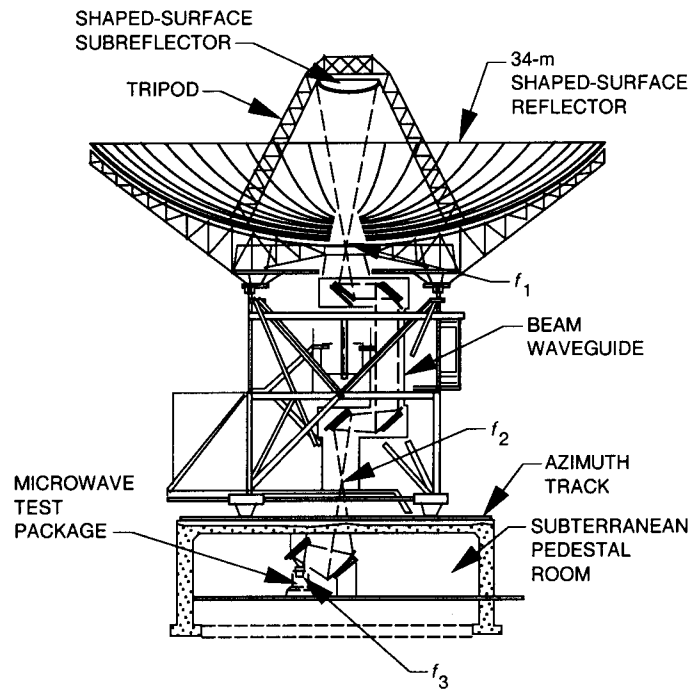
Fig. 1. The 34-meter BWG antenna.
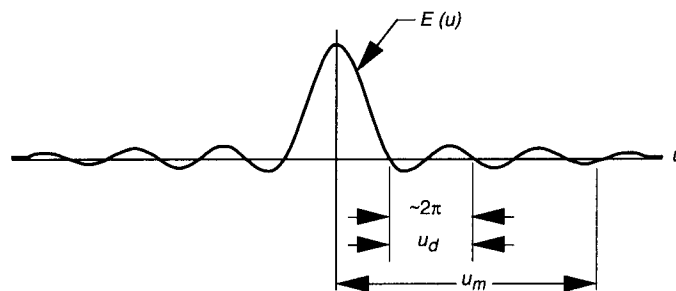
Fig. 2. Application of the sampling theorem.
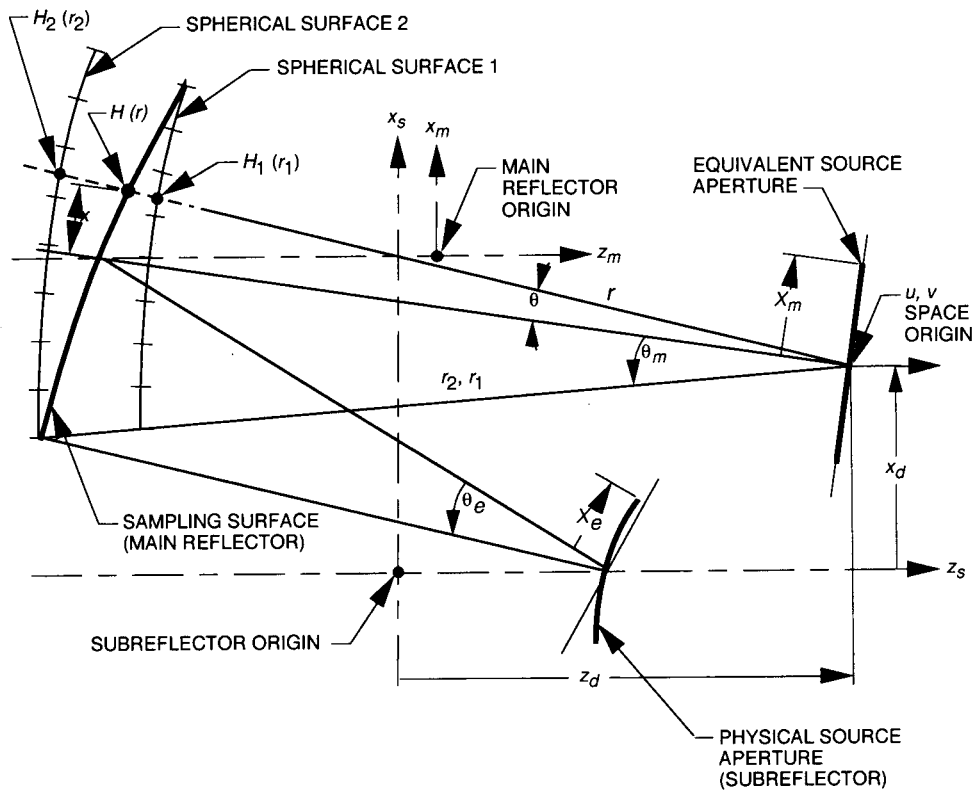
Fig. 3. Interpolation geometry.
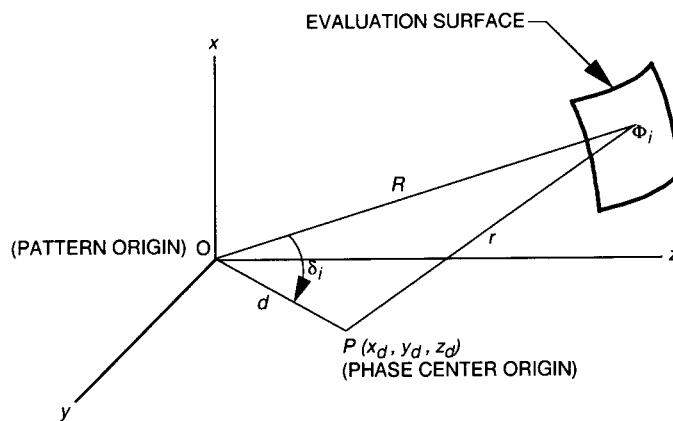
Fig. 4. The phase center algorithm.
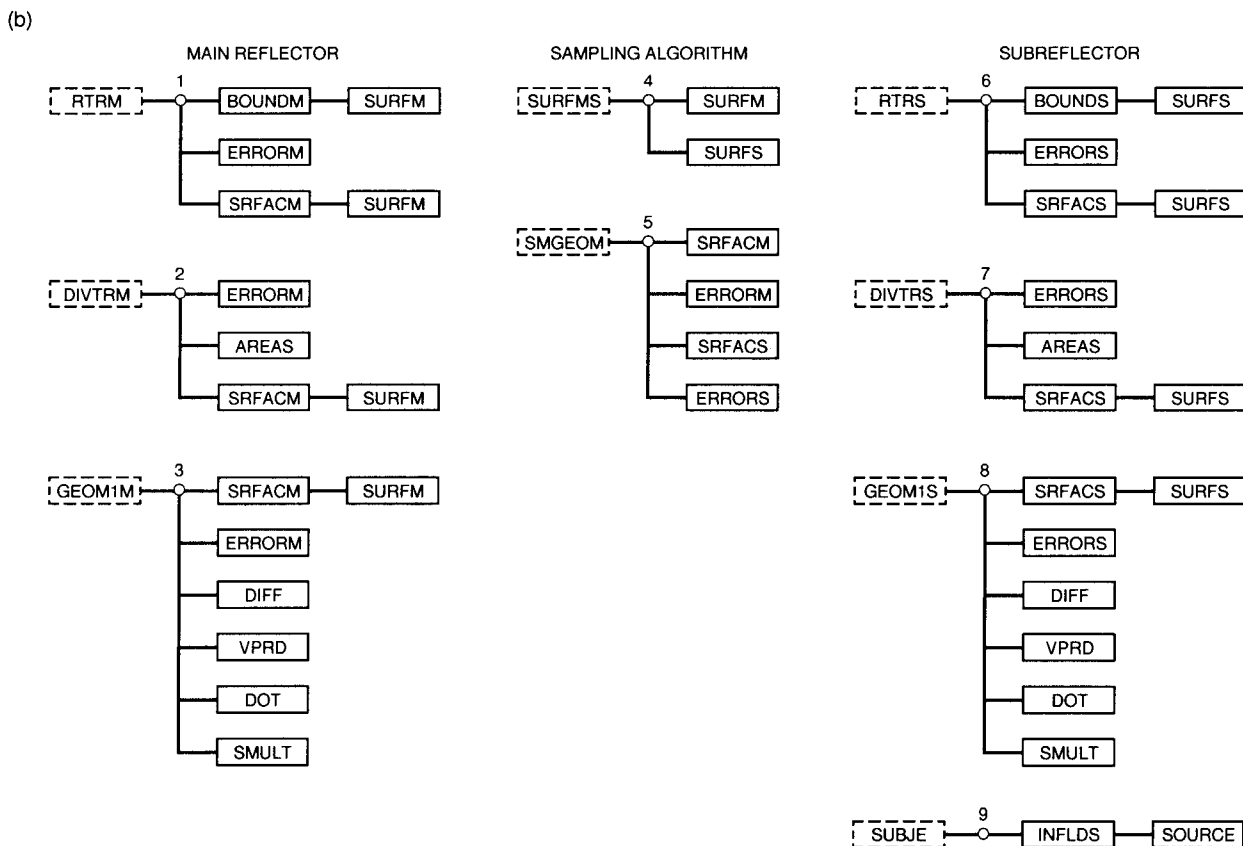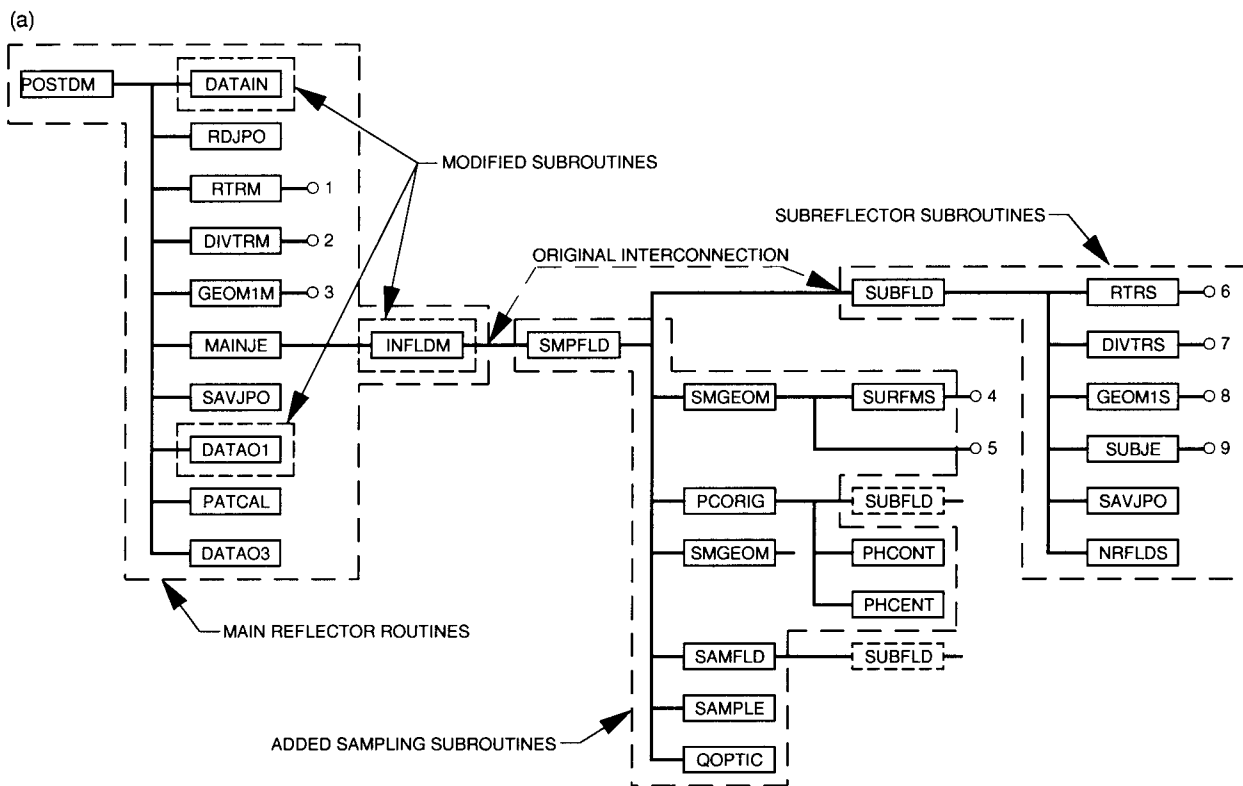
Fig. 5. Organization of the dual-reflector physical optics scattering program with the sampling
algorithm: (a) main routines and (b) lower level routines.

```
                    SAMPLE DATA FILE

FREQ          UNITS
32.0          METERS
XS            YS            ZS
-142.894190 0.0            -217.50
ALPHAS        BETAS         GAMMAS
90.0          120.0         90.0
SCALEM
1.
MFILE
dummy.dat
NDXM          NDYM          XSYMM         YSYMM
270           270           T             F
IFLAGM        SIZEM
-1            1.0
READJE        SAVEJE
f             t
XF            YF            ZF
0.00000       1.75000       0.3710
ALPHAF        BETAF         GAMMAF
0.0           0.0           0.0
SCALES       | SFACT         TFACT         XD           YD           ZD            SUBSW PHASW |
1.           | 0.0           0.0           0.0          0.0          9.0           F     T     |
SFILE
dummy.dat
NDXS          NDYS          XSYMS         YSYMS
340           340           T             F
IFLAGS        SIZES
-1            1.0
CIRPOL        POLX          LHCP
T             F             T
GAIN
0.0
HFILE
f3-22-32.spw
RR
360.0
PHII          PHIF          DPHI
0.0           90.1          90.0
THETAI        THETAF        DTHETA
-16.0         16.1          0.5
THTBPD        PHIBPD
90.           0.
PHSXC         PHSYC         PHSZC
0.0           0.0           260.0
PATNRM
GAIN
POLARZ
SPHERICAL
HFIELD        FRSNEL        ROTATE
F             F             T
PRTPAT        PLTPAT        PLTPHS        WRIT27
F             F             F             T
HFMAGN(1)     HFMAGN(2)     HFMAGN(3)
1.            1.            1.
HFPHN(1)      HFPHN(2)      HFPHN(3)
0.            0.            0.
FLM           DLM           OMEGAM        THDM
130.0         130.0         90.0          10.4
FLS           DLS           OMEGAS        THDS
267.808       370.904       87.753        21.0
```

Fig. 6. Sample input data sheet; added sampling data requirements shown in box.
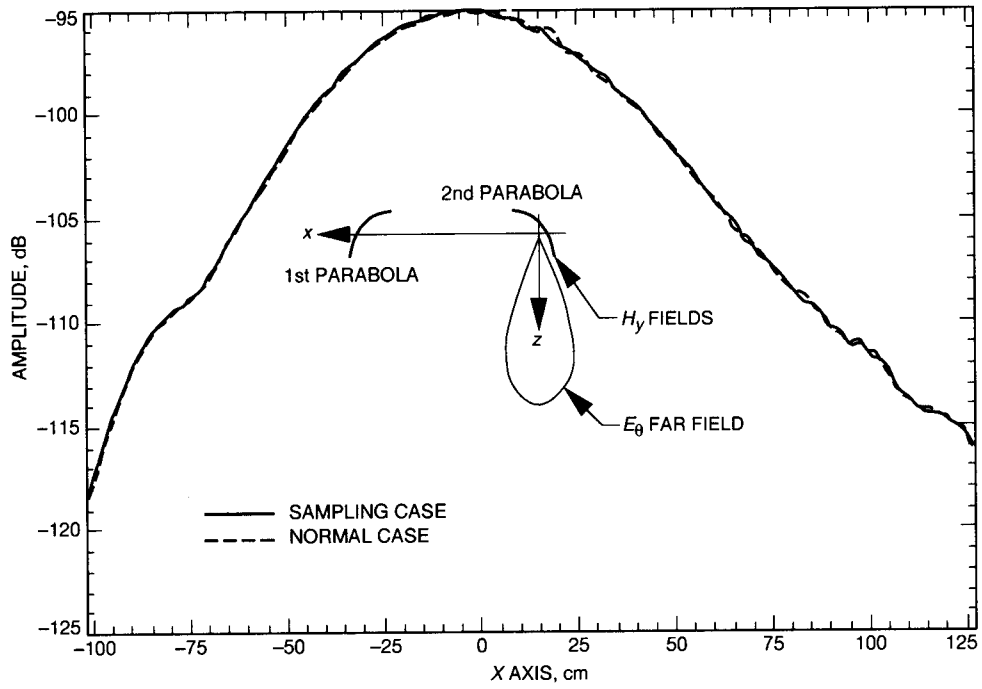
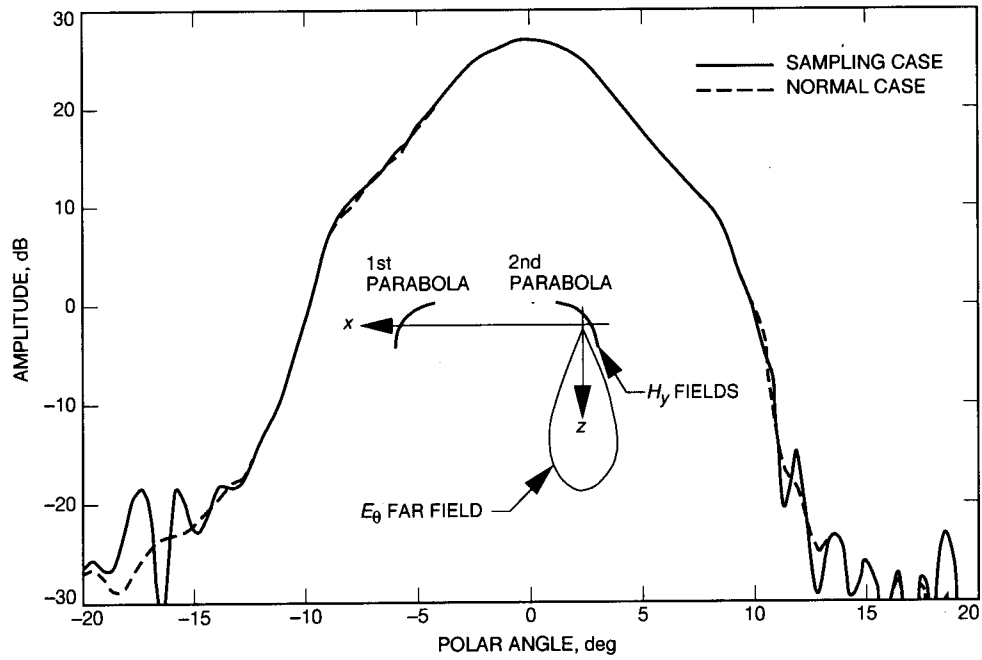Fig. 7. The H_y field on the surface of the second parabola.

Fig. 8. The E_θ far-field component, parabola/parabola.

72

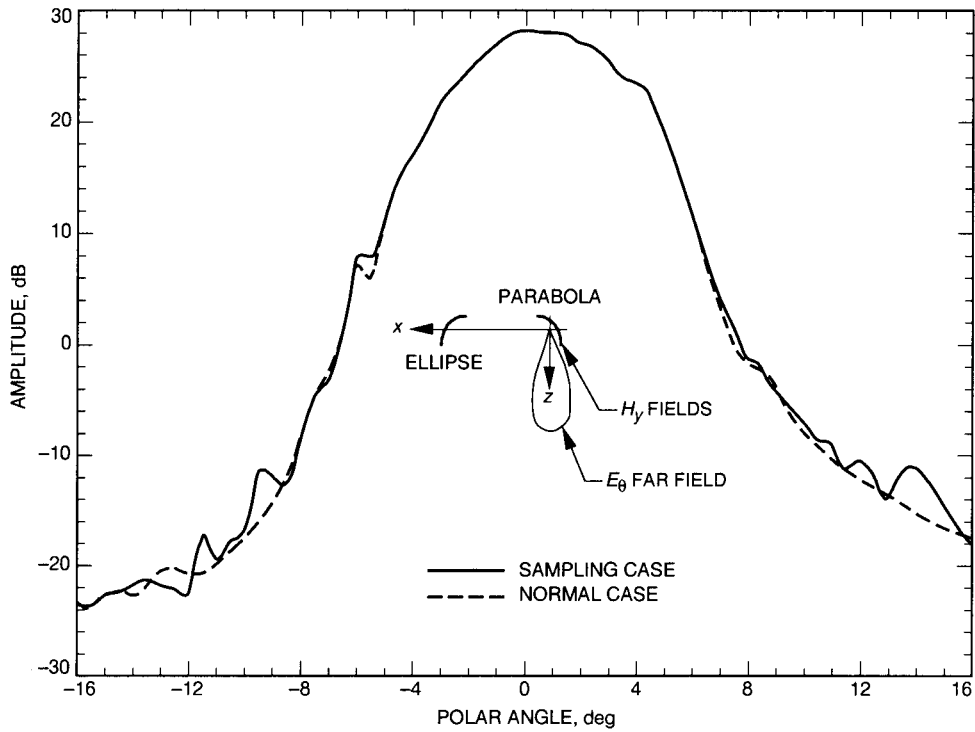Fig. 9. The E_θ far-field component, ellipse/parabola, where the origin
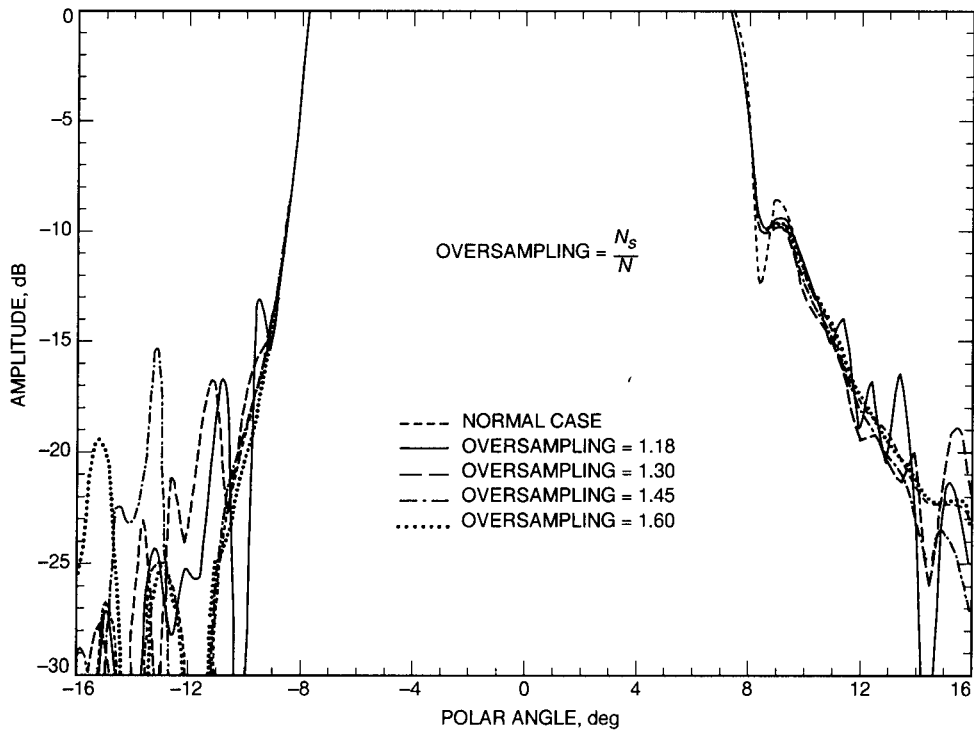for sampling was determined by using the phase center algorithm.

Fig. 10. The effect of sampling resolution, E_θ far-field component,
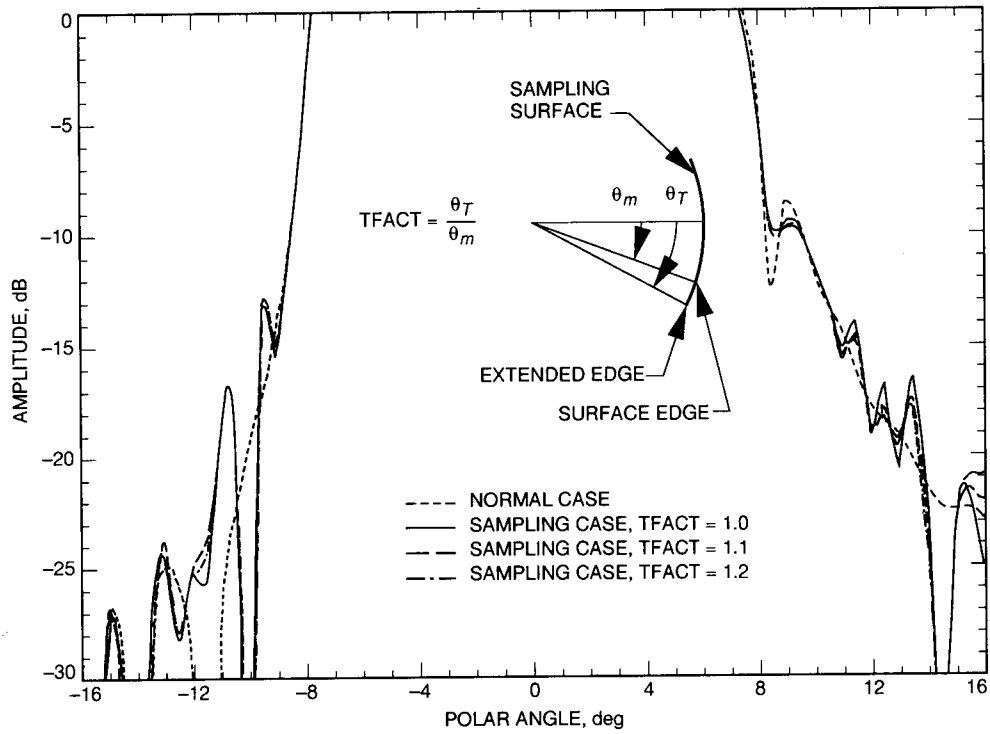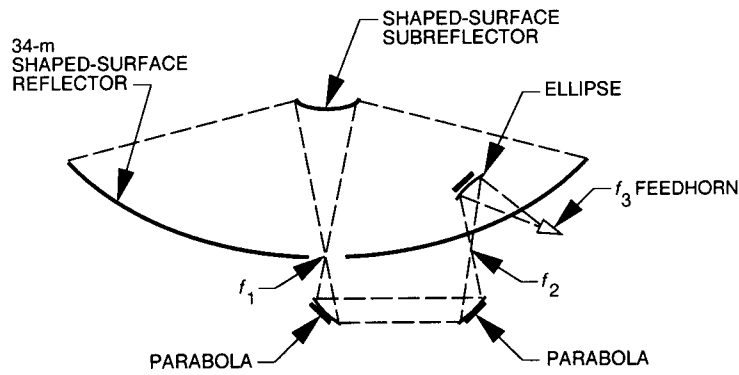ellipse/parabola.

Fig. 11. The effect of increasing the size of the sampling surface, E_θ far-field component, ellipse/parabola.

GEOMETRY	INTEGRATION POINTS PER AXIS 1st/2nd SURFACE	POINTS PER WAVELENGTH	TIME SAMPLING, min	TIME NORMAL, min	TIME RATIO
ELLIPSE/PARABOLA	340/270	1/1	64.43	283.00	4.39
PARABOLA/PARABOLA	270/270	1/1	107.54	181.32	1.69
PARABOLA/SUBREFLECTOR	270/200	1/0.5	32.88	94.72	2.88
SUBTOTAL			204.85 (3.41 hr)	559.04 (9.32 hr)	2.73
SUBREFLECTOR/MAIN	200/24	0.5/··	133.82	133.82	1.00
TOTAL			338.67 (5.64 hr)	692.86 (11.55 hr)	2.05

Fig. 12. Schematic and analysis summary, 34-m BWG antenna, Ka-band.